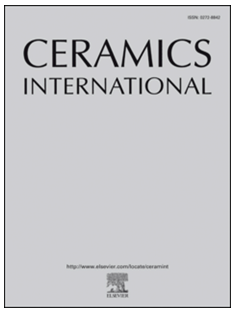

The keys to avoid undesired structural defects in nanotubular TiO_2 films prepared by electrochemical anodization

Martín I. Broens, Wilkendry Ramos Cervantes, Diego Oyarzún Jerez, Manuel López Teijelo, Omar E. Linarez Pérez

PII: S0272-8842(20)30470-3

DOI: https://doi.org/10.1016/j.ceramint.2020.02.145

Reference: CERI 24368

To appear in: *Ceramics International*

Received Date: 6 January 2020

Revised Date: 13 February 2020

Accepted Date: 15 February 2020

Please cite this article as: Martí.I. Broens, W.R. Cervantes, Diego.Oyarzú. Jerez, Manuel.Ló. Teijelo, O.E. Linarez Pérez, The keys to avoid undesired structural defects in nanotubular TiO_2 films prepared by electrochemical anodization, *Ceramics International* (2020), doi: https://doi.org/10.1016/j.ceramint.2020.02.145.

The keys to avoid undesired structural defects in nanotubular TiO_2 films prepared by electrochemical anodization

Martín I. Broens[1,2], Wilkendry Ramos Cervantes[1,2], Diego Oyarzún Jerez[3], Manuel López Teijelo[1,2] and Omar E. Linarez Pérez[1,2,*]

[1]Universidad Nacional de Córdoba. Facultad de Ciencias Químicas. Departamento de Fisicoquímica. Haya de la Torre esq. Medina Allende, X5000HUA. Córdoba, Argentina.

[2]CONICET, INFIQC. Haya de la Torre esq. Medina Allende, X5000HUA. Córdoba, Argentina.

[3]Departamento de Química, Universidad Tecnológica Metropolitana, Av. José Pedro Alessandri 1242, Santiago, Chile.

* Corresponding author:

e-mail address: olinarez@unc.edu.ar (Omar Ezequiel Linarez Pérez)

Abstract

The effect of the viscosity of solvent mixtures based in ethylene glycol on the formation of undesired structural defects (nanograss) during the electrochemical synthesis of nanotubular TiO_2 structures is analyzed. High quality nanotubular TiO_2 films can be achieved by diminishing the viscosity of ethylene glycol-based media by increasing the water content as well as using ethanol as additive. High surface tension of water also promotes the film fracture and accumulation of agglomerates on the film surface. A previously unexplored one-step strategy consisting in the addition of ethanol to ethylene glycol/water mixtures as an alternative anodization medium is proposed. The evidence obtained indicate that this medium allows obtaining nanotubular TiO_2 films with superior structural stability against capillary forces during the film drying, avoiding the use of time consuming post-treatments such as the commonly employed supercritical CO_2 dehydrating, improving the properties of the obtained nanomaterials.

Keywords: Films (A); Anodization (A); Electron microscopy (B); TiO_2 (D)

1. Introduction

For several decades now, nanomaterials have acquired enormous interest due to their exceptional physicochemical properties and large surface area. Among various geometries and chemical nature of nanomaterials, TiO_2 nanotubes (NT-TiO_2) have been the subject of numerous studies due to its semiconductor nature (band-gap ~ 3.0 eV), biocompatibility and photocatalytic activity, between other properties [1,2]. These properties can be enhanced in the nanoscale for their implementation in several applications such as dye sensitized solar cells [3,4], photocathodic protecting films [5], drug-delivery [6], electrochromic devices [7,8], biomedical implants [9,10], gas and biomolecules sensors [11,12] and photocatalysts [13,14].

Due to the wide field of uses, several NT-TiO_2 synthesis methodologies have been studied [15], such as hydrothermal [16,17] and template-assisted [18,19] methods, electrospinning [20,21] and electrochemical routes [22-24]. Electrochemical methods are characterized by its simplicity, low-cost and high control in the morphology of the structures achieved through the conditions of synthesis. In the last decades, many works concerning the anodic formation of NT-TiO_2 films were reported. In this way, it is well-known that it is possible to obtain highly-ordered and oriented NT-TiO_2 films by anodization of titanium in fluoride containing media.

First studies using this methodology involved the use of HF aqueous solutions [22,25] as electrolyte which allowed obtaining NT-TiO_2 films with nanotube lengths lower than or in the order of 1 μm [26,27]. Later, highly viscous organic solvents such as glycerol or ethylene glycol, allowed achieving highly ordered hexagonal NT-TiO_2 arrays with significantly larger nanotubes length (up to 1000 μm) [28-30].

At present, it is considered that TiO_2 films growth takes place by a "high field mechanism" coupled to the TiO_2 chemical dissolution by F^- attack giving Ti(IV) soluble species according to the overall reactions:

$$Ti(s) + 2H_2O(l) \rightarrow TiO_2(s) + 4H^+(aq) + 4e^- \quad (1)$$

$$TiO_2(s) + 6F^-(aq) + 4H^+(aq) \rightarrow TiF_6^{2-}(aq) + 2H_2O(l) \quad (2)$$

Also, some F^- ions incorporation into the TiO_2 phase takes place. The high-field TiO_2 growth occurs by *ionic transport* of species within the TiO_2 phase and the *chemical dissolution* reaction (whatever the high or low value it presents) consumes titanium species that are replenished by further metallic titanium oxidation at the metal/oxide interface due to the high-field mechanism. These main overall reactions describe the *faradaic processes* involving the different titanium species (*ionic current*). Later, several reports from the group of Prof. Xufei Zhu [31-33] have proposed an oxygen bubble mould model due to *electronic current* that leads to oxygen evolution:

$$2H_2O(l) \rightarrow O_2(g) + 4H^+(aq) + 4e^- \quad (3)$$

In this approach, the gas bubbles generated in the electrochemical step 3 could act as tube moulds during coupled the plastic flow of the growing oxide phase [32,34].

From simulation of anodizing current-time curves, they were able to obtain the ionic and electronic current contributions. The oxygen evolution reaction allowed describe the current-time response found in different conditions, but does not correspond to oxidation of titanium species. This, in turn, leads to current efficiencies substantially lower then 1 (based on titanium species), as has been tackled by Schmuki et. al [35] by determining that an important fraction of the total current corresponds to oxygen

evolution. Based on this, ionic current and electronic current are the driving force for barrier oxide growth and oxygen evolution, respectively, where oxygen evolution also plays an important role in the growth of nanotubes. Recent reports employing very different experimental conditions for growth with multiple anodization steps combining potentiostatic/galvanostatic potential programmes, even at potentials where anodization under breakdown takes place argued against the field-assisted dissolution theory [36-39].

Recently, ethanolic based media were employed achieving similar nanotubes structures as those obtained using HF aqueous solutions [40]. Despite of the advantages found using non-aqueous solvents, it has been often found that performing the Ti anodization for several hours or using highly concentrated fluoride media, generates a disordered structure of fibbers or nanotubes debris on the film surface. The grassy appearance of the surface, usually called “nanograss” [28,41,42] or “nanoribbons’ [34], could be a consequence of the non homogeneous chemical dissolution of the nanotube walls. Alternatively, another explanation based on the micro-liquid-flow resulting of the flowing gas from the bottom to the top of the tubes during the anodization, has been given [34]. Furthermore, according to the medium viscosity values, continuous wall thinning takes place generating a partial tubes fragmentation or even the complete collapse of the nanotubular structure as fibbers along the film surface, covering up the nanotube mouths [43]. Nanograss formation has a significant impact on the properties of the material as well as in its further applications. For example, for one-dimensional materials such as TiO_2 nanotubes or nanowires it has been found that the interconnection between them modify the electron transport mechanisms and, consequently, inhibits the charge transfer [44,45]. While this feature has been exploited

for some capacitor-related applications where the large surface area increases the capacitance obtained [46,47], the nanograss formation represents an important limitation for using NT-TiO_2 films in photovoltaic [4,41,45,48] and photocatalysis applications [49,50] due to reduced light absorption, low ionic transport and blockage of the tube mouths access to chemical species. Despite of the effort in this research area, the lack of in situ experimental measurements does not allow obtaining a single accepted mechanism for understanding the NT-TiO_2 films formation and structural defects on their surface.

Different strategies have been proposed in order to obtain nanograss-free NT-TiO_2 films by electrochemical routes that involve mechanical post-treatments for removing the tube fragments such as ultrasound treatments [51] or exfoliation [48]. Despite of their extensive application, these strategies are lack of reproducibility and have undesired effects such as partial or complete detachment of the film from the substrate [52], induction of internal film fractures or a wide-ranging length tube distribution as a result of the inhomogeneity of the operating forces. On the other hand, there have also been reported some strategies focused on the inhibition of the nanograss formation during the anodization procedure, which include the use of protective films [4,53,54], electropolishing pre-treatments that confer to the oxide surface a high resistance to the chemical dissolution [55-57], and the optimization of the synthesis conditions such as applied voltage [58], use of complexing agents [59] or modifying the water content in the electrolytic medium [43]. In relation to the last strategy, the authors have attributed the changes observed in the NT-TiO_2 films morphology to the fluoride ions gradient variation inside the tubes as the viscosity of the electrolytic medium change when the water content is modified [43]. They proposed that a low amount of

water generates large fluoride gradient along the tube length, which promotes the vertical tube splitting by localized chemical etching nearby to their mouths. Contrarily, as the water content increases, the fluoride gradient decreases leading to a homogeneous ring-split along the tubes and then, generating cleaner film surfaces. Despite of this, there is not enough conclusive evidence for explaining the role of the water content in the complex mechanism of nanograss generation.

In this work, we analyze in detail the effect of the electrolytic medium viscosity on nanograss formation in ethylene glycol/water mixtures by modifying either the water content or by using ethanol as a third solvent, keeping constant the water content. The choice of ethanol as additive was based on its similar viscosity to that of water as well as to the analogous chemical structure to that of ethylene glycol. In addition, the effect of capillary forces originated during the drying procedure on the morphology of the obtained nanomaterial, was also analyzed.

2. Materials and methods

Polycrystalline titanium sheets with an exposed geometric area of 0.5 cm^2 (Sigma, 99.7% purity, 0.127 mm thickness) and 10.5 cm^2 (Johnson Matthey Electronics, 99.7% purity, 0.890 mm thickness) were employed as anode and cathode electrodes, respectively. The synthesis of NT-TiO_2 films was carried out using a two-electrode electrochemical cell configuration. The anodization of titanium samples was performed applying a voltage step of 40 V between anode and cathode during 6 h by means of an EG&G PAR model 173 potentiostat/galvanostat (internal power supply of 100 V). Prior to anodizing, the electrodes were degreased by ultrasound treatment in a 50:50 acetone-

ethanol mixture for 30 min and then mounted on Teflon holders. The anodization temperature was fixed at 5°C using a Lauda Alpha cryostat and continuous stirring was applied. A content of 0.8 % w/v ammonium fluoride (Merck, 98% purity) in water/ethylene glycol (W/EG) or water/ethanol/ethylene glycol (W/E/EG) mixtures (Cicarelli, pro-analysis solvents and Milli-Q water) were employed as electrolytic media. For this ammonium fluoride content (0.8 %) an anodizing time of 6 h, which is a typical time where the nanograss develops on the surface of the film, was employed. After the anodization, all samples were copiously rinsed with water. All conditions studied were analyzed from a duplicated set of samples; one of them was dried in air at room temperature, and the other one was immersed consecutively for 2 h in 100:0, 75:25, 50:50, 25:75 and 0:100 water/ethanol and ethanol/acetone mixtures prior to drying with supercritical CO_2 using a BAL-TEC CPD 030 critical point dryer.

Film surface morphology was obtained using a Σigma FESEM Carl Zeiss field-emission scanning electron microscope working at 5 keV gun power, and film thicknesses were determined using a LEXT 3D OLS4000 Olympus confocal microscope (CM) [60]. Single tube geometric features were obtained using a 1200 EXII Jeol transmission electron microscope (TEM) working at 80 keV gun energy. Prior to TEM measurements, the NT-TiO_2 films were dispersed in water by ultrasonic treatment during 30 min and then, a drop of this dispersion was placed on standard Cu grids. In order to determine tubes inner diameter at film surface and oxide film thickness, FESEM and Confocal images analysis were performed using Gwyddion 2.5 software. Statistical measurement of tubes inner diameter from top view FESEM images was carried out considering a high enough number of tubes (N>50) showing clearly visible mouths. Film thickness measurement was performed as been previously detailed [60].

On the other hand, statistical analysis of inner cavity diameters and wall tube thickness from TEM images was performed using ImageJ 1.52q software. Both quantities were measured from a total of 400 points along several (N>20) tube fragments, which present an average length of around 500 nm to 1-2 mm (see Figure 2 and 6 bellow).

Viscosity measurements were performed at 5°C using an MCR 301 Anton Paar Rheoplus Physical rheometer employing a Peltier system with 5 cm in diameter and an 1.006° angle cone-plate configuration. Surface tension measurements were made using the Wilhelmy method at room temperature by means of a Pt plate supported in a KSV Microtrough Langmuir balance (KSV NIMA_Biolin Scientific AB, Västra Frölunda, Sweden).

3. Results and discussion

3.1. Effect of water content

Figure 1 shows top-view FESEM images for NT-TiO_2 films obtained by titanium anodization in ethylene glycol electrolytic media containing 3%, 9% and 15% v/v water, pointing out that there exists an important effect of water content on the film morphology. For low water content (3%), the film surface presents abundant amount of nanograss that hinders the observation and measurement of the nanotubes mouth size (Figs. 1a and b), indicating that a high chemical dissolution of TiO_2 takes place. On the other hand, increasing the water amount to 9% v/v (Figs. 1c and d) or 15% v/v (Figs. 1e and f) produces a significant diminution in nanograss generation, which allows observing a nanograss-free surface with a completely differentiated tubular structure.

Despite of this, for the higher water content employed, nanotubes agglomeration regions delimited by important film fractures are also observed (Figs. 1e and f).

<<Figure 1>>

Regarding the internal structure of single nanotubes, TEM images reflect an important difference in the tubes morphology (Figure 2). It is noticeable that for tubes prepared at low water content (Figs. 2a and b), a gradual increase in the wall thickness from their mouth to the bottom ("V" inner cavity shape morphology). This observation is also qualitatively evidenced in the intensity variations observed in the TEM images for the different conditions explored. Also, for high water content (Figs. 2e and f), the tubes show higher average inner diameter and thinner walls (see Table 1 below), being these morphologic characteristics more uniform along the full tube length in comparison to those obtained using a low water content (Figs. 2a and b).

<<Figure 2>>

Table 1 shows the average and dispersion values of the tubes inner diameter ($d_{i,0}$) measured at the surface from top view FESEM images (Fig. 1), the inner diameter along the tubes length ($d_{i,L}$) and the tube walls thickness (T) obtained by TEM (Fig. 2), as well as the average NT-TiO_2 film thicknesses estimated using Confocal Microscopy [60], which represents approximately the tubes length (L), for nanotubes obtained in different water/ethylene glycol mixtures. The dispersion values for $d_{i,L}$ as well as T, would correspond to changes along the length of the different tube fragments. The average tubes lenght shows a pronounced decrease with the increase in water content, in agreement with the increase in the rate of the oxide chemical dissolution [61]. It is also noticeable that the tubes wall thickness decreases as the viscosity of the electrolyte

decreases, showing a smaller relative dispersion, in agreement with a “V”- to “U”-inner cavity shape transition (Figs 2a-f). In addition, the inner diameter shows a marked increase and the relative dispersion decreases as the water content increases. These observations are also a consequence of the higher and more homogeneous oxide chemical dissolution along the tubes. It has been reported that organic solvents such as glycerol produce a marked increase in the viscosity of the medium, favouring the establishment of high fluoride concentration gradients along the tubes, which thins preferentially the walls in the external oxide region and produce their subsequent longitudinal rupture as nanograss [28,43].

<<Table 1>>

Figure 3 shows the viscosity values measured at 5°C as well as the surface tension values for all the W/EG and W/E/EG mixtures employed. It is noticed that the increase up to 15 %v/v in the water content produces a decrease in viscosity of approximately 32.8% in comparison to the value for a 3 % v/v water mixture (Fig. 3a). According to the surface morphologies obtained (Fig. 1), the water variation chosen is enough to obtain nanograss-free structures for the conditions employed. In this sense, the addition of water in order to decrease the viscosity of the medium reduces the fluoride concentration gradient along the tubes, producing a homogeneous wall thickness in all the channel extension, without showing accumulation of nanograss on the NT-TiO_2 film top surface (Figs 1e,f and Figs 2e,f). Similar results have been reported by varying the anodization temperature, which also modify the viscosity of the medium, but might also generate non-homogeneous oxide film dissolution [62].

<< Figure 3>>

Despite of the beneficial effect observed in the nanotubular structure by lowering the viscosity due to water increase (Fig. 1), the presents results also indicate that addition of water promotes tubes agglomeration and film fracture (see Figs. 1e and f). According to previous studies [45], accumulation of bundled nanotubes may be produced during the titanium anodization as well as during the later solvent evaporation in contact with the film dying medium. These studies, performed with different drying post-treatments in the presence of air, ethanol and supercritical CO_2, have shown that capillary forces that operate during this process generate bending and deflection of the nanotubes, which also depend on the tube geometry (inner and outer diameter, length), the material stiffness and the intrinsic properties of the evaporating solvent (contact angle and surface tension). In addition, the post-treatment using supercritical CO_2 drying allowed obtaining bundle-free and crack-free NT-TiO_2 films [45].

Based in the discussion above, the structural quality of the NT-TiO_2 films may be also determined by the mechanical properties of nanotubes, which depend on their geometrical parameters [63,64]. It has been found that the mechanical behaviour of single TiO_2 nanotubes against axial compression, shows a decrease in the Young modulus of the material as the wall thickness is reduced [65], and then higher tube deflections may take place [45]. This behaviour may be also enhanced by employing very aggressive anodizing conditions, because the increased dissolution rate leads to thinner walls that promote critical points appearance along the tube (see inset in Figure 2f). Then, the local stress at these ultra-thin wall points (< 10 nm) may contribute to the structural collapse of the weakened tubes either by plastic deformation or by cross tube fracture. For the different water/ethylene glycol ratios employed, the measured surface tensions values (Fig. 3b) show a low variation, which is insufficient to explain the

phenomenology obtained (Figs. 1 and 2). Even for the lowest water ratio (3 %v/v), a widespread nanograss effect on the NT-TiO_2 surface is observed (Figs. 1a and b).

In order to obtain high quality NT-TiO_2 surfaces, supercritical CO_2 drying post-treatment has also been employed, even for synthesis conditions that promote nanograss formation [45]. Figure 4 shows top-view FESEM images obtained for NT-TiO_2 surfaces prepared in the same conditions as the films shown in Figure 1, after performing the CO_2 drying treatment as described in the Materials and Methods section. The obtained morphology and trends are similar to those obtained in Figure 1 but showing a significant improvement in terms of the deleterious tubes agglomeration phenomenon. Even for low water content (Figs. 4a and b), the nanograss appearance is different, showing thin tube fragments without agglomeration as those observed in Figure 1a. As water content is increased, the nanotubular TiO_2 surface obtained is nanograss-free and no important agglomeration effects are observed as a direct consequence of the partial inhibition of the lateral deflection forces during the drying process using supercritical CO_2 (Figure 4). In this sense, the drying post-treatment prevents the fragment tubes agglomeration by decreasing drastically the capillary forces in the surface, even when the mechanical properties of the material are not favourable to maintain straight long or thinner tubes in the film structure [29,45]. Despite of these advantages, the main drawback of this procedure is the time-consuming dehydrating steps needed prior to put in contact the NT-TiO_2 films with CO_2 supercritical fluid. In addition, for several characterization techniques, film modification procedures or other specific applications, it could be necessary re-expose the material to different solvents, especially aqueous solutions.

<<Figure 4>>

3.2. Effect of ethanol addition

In order to minimize the nanograss formation by decreasing the viscosity of the electrolytic medium without the addition of high amounts of water, different ethanol additions to the W/EG mixture with 3% water taken as a reference, were analyzed. Figure 3a shows the measured viscosity at 5°C for ethanol contents in the range of 6-20% v/v maintaining the water content as low as possible (3 % v/v). It is noticed that the ethanol addition leads to a decrease in the viscosity of the medium up to approximately 38.9% for the highest ethanol content (20%) mixture (3:20:77), which is similar to the obtained for the higher water content employed (15 %v/v).

Figure 5 shows top-view FESEM images of NT-TiO_2 films synthesized using the different W/E/EG mixtures. For the lowest ethanol content (3:6:91 mixture), less nanograss formation is observed at the film surface (Figs. 5a and b) in comparison to the obtained using the same water content in the non-ethanolic medium (Figs. 1a and b). Also, as the ethanol content is increased up to 20% v/v, a significantly cleaner nanotubular TiO_2 surface free of nanograss is obtained, showing well-defined mouths without tubes agglomeration (Figs. 5c-f). In addition, for the 20 % v/v ethanol addition (Figs. 5e and f), the tubes are well ordered and symmetric showing homogeneous diameters throughout the full surface in comparison to those obtained using high water content (Figs. 1e and f) or after supercritical CO_2 drying in the same anodizing conditions (Figs. 4e and f). These evidences clearly indicate that the use of low viscosity media is required to obtain nanograss-free NT-TiO_2 surfaces for ethylene glycol-based electrolytes with high fluoride ions concentration (0.8 % w/v).

<<Figure 5>>

Figure 6 shows TEM images obtained for the NT-TiO_2 films anodized in the selected W/E/EG mixtures and Table 2 summarizes the overall morphological features (inner diameter at film surface and along the tubes extent, tubes wall and tubes lenght). Similarly to the trends obtained as water content is increased (see Table 1), there is a decrease in the tubes wall thickness and an increase in the inner diameter as well as a decrease in the film thickness as the ethanol content is increased (Table 2). These trends are attributed to a higher transport of chemical species due to the decrease in viscosity. This generates both a higher oxide chemical dissolution rate, which explain the tendencies observed, and a moderate fluoride gradient along the tubes that leads to a more homogeneous chemical dissolution observed as a transition from "V" (Figs. 6a and b) to "U" (Figs. 6e and f) inner cavity shapes.

<<Figure 6>>

<<Table 2>>

In addition, variation of the different geometric parameter values listed in Table 1 (water content effect) are more pronounced that those shown in Table 2 (ethanol content effect). For example, despite that the 15:85 non-ethanolic and the 3:20:77 ethanolic mixture have similar viscosity values (Fig. 3a), thinner walls and shorter tubes are obtained in the non-ethanolic medium. These results would indicate that the increase in the chemical dissolution rate is greater when viscosity is changed by increasing water content in comparison to the addition of ethanol due to a better solvation of chemical species. Consequently, more fragile and susceptible to fracture are the NT-TiO_2 films obtained. Contrarily, the use of ethanol-containing media produces thicker tube walls leading to more stable films against lateral deflection effects and minimizing the

capillary forces due to decrease the surface tension of the medium (see Figure 3b). These promising characteristics confer important advantages to this synthesis strategy since additional post-treatments steps are not required (see schematic representation in Figure 7).

<<Figure 7>>

In summary, we have shown that high quality NT-TiO_2 films can be easily achieved by diminishing the viscosity of ethylene glycol-based medium by increasing water content as well as using ethanol as additive. We demonstrate that water content affects directly the oxide film dissolution rate generating a more homogeneous concentration gradient of fluoride along the tubes. This effect clearly produces both nanograss-free surfaces and "U"-inner cavity shape morphology along the tubes (Figs. 2 and 7), similarly to nanotubular TiO_2 films obtained using HF aqueous media [66]. However, too high water content leads to fragile and fracturable films due to the thin walls of the tubes. In this regard, the addition of ethanol to the anodization medium maintaining a low water content in highly fluoride-containing electrolytes allows obtaining nanograss-free NT-TiO_2 films with greater structural stability against capillary forces (Fig. 7).

4. Conclusions

The effect of the viscosity in ethylene glycol/water mixtures on nanograss formation during titanium anodization in fluoride-containing media has been studied. The evidences obtained indicate that the nanograss formation can be controlled by regulating the viscosity of the electrolyte. The decrease in the viscosity by adding a

solvent with low intrinsic viscosity and similar chemical structure to the base ethylene glycol solvent such as ethanol, promotes both the homogeneous chemical dissolution along the tubes length as well as the inhibition of fractures and tubes agglomeration on the film surface.

The one-step strategy proposed allows obtaining nanograss-free nanotubular TiO_2 films, avoiding the use of time consuming post-treatments such as supercritical CO_2 drying. This, in turn, produces structural high-quality materials for further applications.

Acknowledgments

We thank the financial support by SECYT-UNC and CONICET. M.I.B. and W.R.C thank CONICET for the fellowships granted. FESEM and TEM microscopy facilities at LAMARX (FAMAF-UNC) and CIAP-INTA, Sistema Nacional de Microscopía–MINCyT, are gratefully acknowledged. The authors also thank Dr. César G. Gómez and Dr. Miriam C. Strumia (IPQA-CONICET-UNC) for viscosity measurements and Dr. Soledad Bazán (Dpto. Química Biológica Ranwel Caputto- CIQUIBIC-CONICET-UNC) for surface tension values.

Author contributions

The manuscript was written through contributions of all authors. All authors have given approval to the final version of the manuscript.

References

[1] K. Lee, A. Mazare, P. Schmuki, One-dimensional titanium dioxide nanomaterials: Nanotubes, Chem. Rev. 114 (2014) 9385–9454. https://doi.org/10.1021/cr500061m

[2] P. Roy, S. Berger, P. Schmuki, TiO_2 nanotubes: Synthesis and applications, Angew. Chem. Int. Ed. 50 (2011) 2904–2939. https://doi.org/10.1002/anie.201001374

[3] J. M. Macák, H. Tsuchiya, A. Ghicov, P. Schmuki, Dye-sensitized anodic TiO_2 nanotubes, Electrochem. Commun. 7 (2005) 1133–1137. https://doi.org/10.1016/j.elecom.2005.08.013

[4] P. Roy, S. P. Albu, P. Schmuki, TiO_2 nanotubes in dye-sensitized solar cells: Higher efficiencies by well-defined tube tops, Electrochem. Commun. 12 (2010) 949–951. https://doi.org/10.1016/j.elecom.2010.04.029

[5] J. Zhang, J. Hu, Y.-F. Zhu, Q. Liu, H. Zhang, R.-G. Du, C.-J. Lin, Fabrication of CdTe/ZnS core/shell quantum dots sensitized TiO_2 nanotube films for photocathodic protection of stainless steel, Corros. Sci. 99 (2015) 118-124. https://doi.org/10.1016/j.corsci.2015.06.029

[6] C. Moseke, F. Hage, E. Vorndran, U. Gbureck, TiO_2 nanotube arrays deposited on Ti substrate by anodic oxidation and their potential as a long-term drug delivery system for antimicrobial agents, Appl. Surf. Sci. 258 (2012) 5399-5404. https://doi.org/10.1016/j.apsusc.2012.02.022

[7] A. Ghicov, H. Tsuchiya, R. Hahn, J. M. Macak, A. G. Muñoz, P. Schmuki, TiO_2 nanotubes: H^+ insertion and strong electrochromic effects, Electrochem. Commun. 8 (2006) 528–532. (2006) 528–532. https://doi.org/10.1016/j.elecom.2006.01.015

[8] S. Berger, A. Ghicov, Y. C. Nah, P. Schmuki, Transparent TiO_2 nanotube electrodes via thin layer anodization: Fabrication and use in electrochromic devices, Langmuir 25 (2009) 4841–4844. https://doi.org/10.1021/la9004399

[9] A. Kar, K. S. Raja, M. Misra, Electrodeposition of hydroxyapatite onto nanotubular TiO_2 for implant applications, Surf. Coat. Tech. 201 (2006) 3723–3731. https://doi.org/10.1016/j.surfcoat.2006.09.008

[10] C. von Wilmowsky, S. Bauer, R. Lutz, M. Meisel, F. W. Neukam, T. Toyoshima, P. Schmuki, E. Nkenke, K. A. Schlegel, In vivo evaluation of anodic TiO_2 nanotubes: An experimental study in the pig, J. Biomed. Mater. Res. 89B (2009) 165–171. https://doi.org/10.1002/jbm.b.31201

[11] O. K. Varghese, D. Gong, M. Paulose, K. G. Ong, C. A. Grimes, Hydrogen sensing using titania nanotubes, Sens. Actuators B: Chem. 93 (2003) 338–344. https://doi.org/10.1016/S0925-4005(03)00222-3

[12] M. Terracciano, V. Galstyan, I. Rea, M. Casalino, L. De Stefano, G. Sbervegleri, Chemical modification of TiO_2 nanotube arrays for label-free optical biosensing applications, Appl. Surf. Sci. 419 (2017) 235-240. https://doi.org/10.1016/j.apsusc.2017.05.029

[13] S. P. Albu, A. Ghicov, J. M. Macak, R. Hahn, P. Schmuki, Self-organized, free-standing TiO_2 nanotube membrane for flow-through photocatalytic applications, Nano Lett. 7 (2007) 1286–1289. https://doi.org/10.1021/nl070264k

[14] J. M. Macak, M. Zlamal, J. Krysa, P. Schmuki, Self-organized TiO_2 nanotube layers as efficient highly photocatalysts, Small 3 (2007) 300–304. https://doi.org/10.1002/smll.200600426

[15] Y. L. Pang, S. Lim, H. C. Ong, W. T. Chong, A critical review on the recent progress of synthesizing techniques and fabrication of TiO_2-based nanotubes photocatalysts, Appl. Catal. A: Gen. 481 (2014) 127–142. https://doi.org/10.1016/j.apcata.2014.05.007

[16] T. Kasuga, M. Hiramatsu, A. Hoson, T. Sekino, K. Niihara, Formation of titanium oxide nanotube, Langmuir 14 (1998) 3160–3163. https://doi.org/10.1021/la9713816

[17] B. D. Yao, Y. F. Chan, X. Y. Zhang, W. F. Zhang, Z. Y. Yang, N. Wang, Formation mechanism of TiO_2 nanotubes. Appl. Phys. Lett. 82 (2003) 281–283. https://doi.org/10.1063/1.1537518

[18] P. Hoyer, Formation of a titanium dioxide nanotube array, Langmuir 12 (1996) 1411–1413. https://doi.org/10.1021/la9507803

[19] H. Shin, D. K. Jeong, J. Lee, M. M. Sung, J. Kim, Formation of TiO_2 and ZrO_2 Nanotubes Using Atomic Layer Deposition with Ultraprecise Control of the Wall Thickness, Adv. Mater. 16 (2004) 1197–1200. https://doi.org/10.1002/adma.200306296

[20] D. Li, Y. Xia, Direct fabrication of composite and ceramic hollow nanofibers by electrospinning, Nano Lett. 4 (2004) 933–938. https://doi.org/10.1021/nl049590f

[21] C. Lopez de Dicastillo, C. Patiño, M. J. Galotto, J. L. Palma, D. Alburquenque, J. Escrig, Novel antimicrobial titanium dioxide nanotubes obtained through a combination

of atomic layer deposition and electrospinning technologies, Nanomaterials 8 (2018) 128-145. https://doi.org/10.3390/nano8020128

[22] D. Gong, C. A. Grimes, O. K. Varghese, W. Hu, R. S. Singh, Z. Chen, E. C. Dickey, Titanium oxide nanotube arrays prepared by anodic oxidation, J. Mater. Res. 16 (2001) 3331–3334. https://doi.org/10.1557/JMR.2001.0457

[23] J. M. Macak, A. Ghicov, K. Yasuda, R. Hahn, S. Bauer, P. Schmuki, TiO_2 nanotubes: Self-organized electrochemical formation, properties and applications, Curr. Opin. Solid St. Mat. 11 (2007) 3–18. https://doi.org/10.1016/j.cossms.2007.08.004

[24] A. Ghicov, P. Schmuki, Self-ordering electrochemistry: a review on growth and functionality of TiO_2 nanotubes and other self-aligned MO_x structures, Chem. Commun. (2009) 2791-2808. https://doi.org/10.1039/b822726h

[25] V. Zwilling, E. Darque-Ceretti, A. Boutry-Forveille, D. David, M. Y. Perrin, M. Aucouturier, Structure and physicochemistry of anodic oxide films on titanium and TA6V alloy, Surf. Interface Anal. 27 (1999) 629-637. https://doi.org/10.1002/(SICI)1096-9918(199907)27:7<629::AID-SIA551>3.0.CO;2-0

[26] R. Beranek, H. Hildebrand, P. Schmuki, Self-organized porous titanium oxide prepared in H_2SO_4-HF electrolytes, Electrochem. Solid-State Lett. 6 (2003**)** B12-B14. https://doi.org/10.1149/1.1545192

[27] S. Bauer, S. Kleber, P. Schmuki, TiO_2 nanotubes: Tailoring the geometry in H_3PO_4/HF electrolytes, Electrochem. Commun. 8 (2006) 1321–1325. https://doi.org/10.1016/j.elecom.2006.05.030

[28] J. M. Macak, P. Schmuki, Anodic growth of self-organized anodic TiO_2 nanotubes in viscous electrolytes, Electrochim. Acta 52 (2006) 1258–1264. https://doi.org/10.1016/j.electacta.2006.07.021

[29] M. Paulose, H. E. Prakasam, O. K. Varghese, L. Peng, K. C. Popat, G. K. Mor, T. A. Desai, C. A. Grimes, TiO_2 nanotube arrays of 1000 μm length by anodization of titanium foil: Phenol red diffusion, J. Phys. Chem. C 111 (2007) 14992–14997. https://doi.org/10.1021/jp075258r

[30] Z. Jing-zhong, B. Yang, Z. Kun, L. Ye, K. Lu, Preparation of separated and open end TiO_2 nanotubes, Ceram. Int. 41 (2015) 7235–7240. https://doi.org/10.1016/j.ceramint.2015.02.157

[31] Y. Ruiquan, J. Longfei, Z. Xufei, S. Ye, Y. Dongliang, H. Aijun, Theoretical derivation of ionic current and electronic current and comparison between fitting curves and measured curves, RSC. Adv. 2 (2012) 12474-12481. https://doi.org/10.1039/c2ra22124a

[32] B. Chong, D. Yu, R. Jin, Y. Wang, D. Li, Y. Song, M. Gao, X. Zhu, Theoretical derivation of anodizing current and comparison between fitted curves and measured curves under different conditions, Nanotechnology 26 (2015) 145603. https://doi.org/10.1088/0957-4484/26/14/145603

[33] S. Chen, M. Liao, P. Yang, S. Yan, R. Jin, X. Zhu, Simulation of anodizing current-time curves and the morphology evolution of TiO_2 nanotubes obtained in phosphoric electrolytes, RSC Adv. 6 (2016) 84309-84318. https://doi.org/10.1039/c6ra17125g

[34] S. Zhang, S. Xu, D. Hu, C. Zhang, J. Che, Y. Song, Formation of TiO_2 nanoribbons by anodization under high current density, Mater. Res. Bull. 103 (2018) 205-210. https://doi.org/10.1016/j.matersbull.2018.02.014

[35] S. P. Albu, N. Taccardi, I. Paramasivam, K. R. Hebert, P. Schmuki, Oxide growth efficiencies and self-organization of TiO_2, J. Electrochem. Soc. 159 (2012) H697-H703. https://doi.org/10.1149/2.015208jes

[36] K. Zhang, S.K. Cao, C. Li, J. Qi, L.F. Jiang, J. Zhang, X.F. Zhu, Rapid growth of TiO_2 nanotubes under the compact oxide layer: Evidence against the digging manner of dissolution reaction, Electrochemistry Communications 103 (2019) 88-93. https://doi.org/10.1016/j.elecom.2019.05.015

[37] W.Q. Huang, H.Q. Xu, Z.R. Ying, Y. Dan, Q. Zhou, J. Zhang, X.F. Zhu, Split TiO_2 nanotubes - Evidence of oxygen evolution during Ti anodization, Electrochemistry Communications 106 (2019) 106532. https://doi.org/10.1016/j.eliecom.2019.106532

[38] J.J. Zhang, W.Q. Huang, K. Zhang, D.Z. Li, H.Q. Xu, X.F. Zhu, Bamboo shoot nanotubes with diameters increasing from top to bottom: Evidence against the field-assisted dissolution equilibrium theory, Electrochemistry Communications 100 (2019) 48-51. https://doi.org/10.1016/j.elecom.2019.01.019

[39] M.S. Yu, Y. Chen, C. Li, S. Yan, H.M. Cui, X.F. Zhu, J.S. Kong, Studies of oxide growth location on anodization of Al and Ti provide evidence against the field-assisted dissolution and field-assisted ejection theories, Electrochemistry Communications 87 (2018) 76-80. https://doi.org/10.1016/j.elecom.2018.01.003

[40] M. Michalska-Domasska, P. Nyga, M. Czerwi-ski, Ethanol-based electrolyte for nanotubular anodic TiO_2 formation. Corros. Sci. 134 (2018) 99–102. https://doi.org/10.1016/j.corsci.2018.02.012

[41] D. Kim, A. Ghicov, P. Schmuki, TiO_2 Nanotube arrays: Elimination of disordered top layers ("nanograss") for improved photoconversion efficiency in dye-sensitized solar cells, Electrochem. Commun. 10 (2008) 1835–1838. https://doi.org/10.1016/j.elecom.2008.09.029

[42] Q. Chen, H. Liu, Y. Xin, X. Cheng, J. Zhang, J. Li, P. Wang, H. Li, Controlled anodic growth of TiO_2 nanobelts and assessment of photoelectrochemical and photocatalytic properties, Electrochim. Acta 99 (2013) 152–160. https://doi.org/10.1016/j.electacta.2013.03.032

[43] J. Naduvath, P. Bhargava, S. Mallick, Mechanism of titania nanograss formation during anodization, Chem. Phys. Lett. 626 (2015) 15–19. https://doi.org/10.1016/j.cplett.2015.03.011

[44] J. A. Frank, N. Kopidakis, J. van de Lagemaat, Electrons in nanostructured TiO_2 solar cells: transport, recombination and photovoltaic properties, Coord. Chem. Rev. 248 (2004) 1165–1179. https://doi.org/10.1016/j.ccr.2004.03.015

[45] K. Zhu, T. B. Vinzant, N. R. Neale, A. J. Frank, Removing structural disorder from oriented TiO_2 nanotube arrays: Reducing the dimensionality of transport and recombination in dye-sensitized solar cells, Nano Lett. 7 (2007) 3739–3746. https://doi.org/10.1021/nl072145a

[46] K. Du, G. Liu, M. Li, C. Wu, X. Chen, K. Wang, Electrochemical reduction and capacitance of hybrid titanium dioxides-nanotube arrays and "nanograss", Electrochim. Acta 210 (2016) 367–374. https://doi.org/10.1016/j.electacta.2016.05.027

[47] S. Zhao, Y. Chen, Z. Zhao, L. Jiang, C. Zhang, J. Kong, X. Zhu, Enhanced capacitance of TiO_2 nanotubes topped with nanograss by H_3PO_4 soaking and hydrogenation doping, Electrochim. Acta 266 (2018) 233–241. https://doi.org/10.1016/j.electacta.2018.02.037

[48] Y. Liao, D. Zhang, Q. Wang, T. Wen, K. Jia, Z. Zhong, F. Bai, L. Tang, W. Que, H. Zhang, Open-top TiO_2 nanotube arrays with enhanced photovoltaic and photochemical performances via a micromechanical cleavage approach, J. Mater. Chem. 3 (2015), 14279–14283. https://doi.org/10.1039/c5ta02799c

[49] A. Mazzarolo, K. Lee, A. Vicenzo, P. Schmuki, Anodic TiO_2 nanotubes: Influence of top morphology on their photocatalytic performance, Electrochem. Commun. 22 (2012) 162–165. https://doi.org/10.1016/j.elecom.2012.05.037

[50] G. Cha, K. Lee, J. Yoo, M. S. Killian, P. Schmuki, Topographical study of TiO_2 nanostructure surface for photocatalytic hydrogen production, Electrochim. Acta 179 (2015) 423–430. https://doi.org/10.1016/j.electacta.2015.02.127

[51] J. Wang, Z. Lin, Freestanding TiO_2 nanotube arrays with ultrahigh aspect ratio via electrochemical anodization, Chem. Mater. 20 (2008) 1257–1261. https://doi.org/10.1021/cm7028917

[52] H. Xu, Q. Zhang, C. Zheng, W. Yan, W. Chu, Application of ultrasonic wave to clean the surface of the TiO_2 nanotubes prepared by the electrochemical anodization, Appl. Surf. Sci. 257 (2011) 8478-8480. https://doi.org/10.1016/j.apsusc.2011.04.135

[53] Y. Y. Song, R. Lynch, D. Kim, P. Roy, P. Schmuki, TiO_2 nanotubes: Efficient suppression of top etching during anodic growth, Electrochem. Solid-State Lett. 12 (2009) C17-C20. https://doi.org/10.1149/1.3126500

[54] Q. Gui, D. Yu, D. Li, Y. Song, X. Zhu, L. Cao, S. Zhang, W. Ma, S. You, Efficient suppression of nanograss during porous anodic TiO_2 nanotubes growth. Appl. Surf. Sci. 314 (2014) 505–509. https://doi.org/10.1016/j.apsusc.2014.07.046

[55] D. Kim, A. Ghicov, P. Schmuki, TiO_2 Nanotube arrays: Elimination of disordered top layers ("nanograss") for improved photoconversion efficiency in dye-sensitized solar cells, Electrochem. Commun. 10 (2008) 1835–1838. https://doi.org/10.1016/j.elecom.2008.09.029

[56] V. Asgari, M. Noormohammadi, A. Ramazani, M. A. Kashi, A new approach to electropolishing of pure Ti foil in acidic solution at room temperature for the formation of ordered and long TiO_2 nanotube arrays, Corros. Sci. 136 (2018) 38-46. https://doi.org/10.1016/j.corsci.2018.02.040

[57] A. Pourandarjani, F. Nasirpouri, Tuning substrate roughness to improve uniform growth and photocurrent response in anodic TiO_2 nanotube arrays, Ceram. Int. 44 (2018) 22671-22679. https://doi.org/10.1016/j.ceramint.2018.09.045

[58] H. Fraoucene, D. Hatem, F. Vacandio, M. Pasquinelli, TiO_2 nanotubes with nanograss structure: The effect of the anodizing voltage on the formation mechanism

and structure properties, J. Electron, Mater. 48 (2019) 2046–2054. https://doi.org/10.1007/s11664-019-06951-y

[59] F. Bonatto, J. Venturini, A. C. Frantz, T. C. L. dos Santos, C. P. Bergmann, A. G. Brolo, One-step synthesis of nanograss-free TiO_2 nanotubes using DTPA-enriched electrolytes, Ceram. Int. 44 (2018) 22345–2235. https://doi.org/10.1016/j.ceramint.2018.08.360

[60] D. P. Oyarzún, O. E. Linarez Pérez, M. López Teijelo, C. Zúñiga, E. Jeraldo, D. A. Geraldo, R. Arratia-Perez, Atomic force microscopy (AFM) and 3D confocal microscopy as alternative techniques for the morphological characterization of anodic TiO_2 nanoporous layers, Mater. Lett. 165 (2016) 67–70. https://doi.org/10.1016/j.matlet.2015.11.087

[61] S. Berger, J. Kunze, P. Schmuki, A. T. Valota, D. J. LeClere, P. Skeldon, G. E. Thompson, Influence of water content on the growth of anodic TiO_2 nanotubes in fluoride-containing ethylene glycol electrolytes, J. Electrochem. Soc. 157 (2010) C18-C23. https://doi.org/10.1149/1.3251338

[62] J. Chen, J. Lin, X. Chen, Self-assembled TiO_2 nanotube arrays with U-shaped profile by controlling anodization temperature, J. Nanomater. (2010) 753253-753257. https://doi.org/10.1155/2010/753253

[63] N. G. Chopra, L. X. Benedict, V. H. Crespi, M. L. Cohen, S. G. Louie, A. Zettl, Fully collapsed carbon nanotubes, Nature 377 (1995) 135–138. https://doi.org/10.1038/377135a0

[64] X. Yu, Z. Zhan, The effects of the size of nanocrystalline materials on their thermodynamic and mechanical properties, Nanoscale Res. Lett. 9 (2014) 516-522. https://doi.org/10.1186/1556-276X-9-516

[65] T. Shokuhfar, G. K. Arumugam, P. A. Heiden, R. S. Yassar, C. Friedrich, Direct compressive measurements of individual titanium nano dioxide tubes, ACS Nano 3 (2009) 3098–3102. https://doi.org/10.1021/nn900202x

[66] J. E. Yoo, P. Schmuki, Critical factors in the anodic formation of extremely ordered titania nanocavities, J. Electrochem. Soc. 166 (2019) C3389–C3398. https://doi.org/10.1149/2.0381911jes

Captions for figures and tables

Figure 1. Top-view FESEM images for NT-TiO_2 films grown at 5°C applying a voltage step of 40 V during 6 h in 0.8 % w/v NH_4F + x % v/v water + (100-x) % v/v ethylene glycol electrolyte. x: 3 (a and b); 9 (c and d) and 15 (e and f).

Figure 2. TEM images for NT-TiO_2 films grown at 5°C applying a voltage step of 40 V during 6 h in 0.8 % w/v NH_4F + x % v/v water + (100-x) % v/v ethylene glycol electrolyte. x: 3 (a and b); 9 (c and d) and 15 (e and f). Inset in Fig. 2f shows the presence of critical points along the tube extension.

Figure 3. Viscosity at 5°C (a) and surface tension at room temperature (b) for the water/ethylene glycol and water/ethanol/ethylene glycol mixtures employed.

Figure 4. Top view FESEM images for NT-TiO_2 films grown at 5°C applying a voltage step of 40 V during 6 h in 0.8 % w/v NH_4F + x % v/v water + (100-x) % v/v ethylene glycol electrolyte after supercritical CO_2 drying post-treatment. x: 3 (a and b); 9 (c and d) and 15 (e and f).

Figure 5. Top view FESEM images for NT-TiO_2 films grown at 5°C applying a voltage step of 40 V during 6 h in 0.8 % w/v NH_4F + 3 % v/v water + x % v/v ethanol + (97-x) % v/v ethylene glycol electrolyte. x: 6 (a and b); 12 (c and d) and 20 (e and f).

Figure 6. TEM images for NT-TiO_2 films grown at 5°C applying a voltage step of 40 V during 6 h in 0.8 % w/v NH_4F + 3 % v/v water + x % v/v ethanol + (97-x) % v/v ethylene glycol electrolyte. x: 6 (a and b); 12 (c and d) and 20 (e and f).

Figure 7. Schematic representation of the effect of anodization medium viscosity on the pore wall thickness.

Table 1. Geometric parameters for NT-TiO_2 films obtained using different water content in the anodizing medium.

Table 2. Geometric parameters for NT-TiO_2 films obtained using different ethanol content in the anodizing medium maintaining a 3 % v/v of water.

Table 1

Water/Ethylene glycol mixture	Inner diameter at film surface ($d_{i,0}$) /nm [(a)]	Inner diameter along the tubes lenght ($d_{i,L}$) /nm [(b)]	Tube wall thickness (T) /nm [(b)]	Tubes length (L) /μm [(c)]
3:97	77 ± 4	69 ± 24	38 ± 15	6.7 ± 0.8
9:91	82 ± 11	79 ± 13	26 ± 6	5.5 ± 0.6
15:85	110 ± 10	114 ± 13	12 ± 4	4.4 ± 0.7

[(a)] From top-view FESEM images

[(b)] From TEM images

[(c)] From Confocal microscopy analysis

Table 2

Water/Ethanol/ Ethylene glycol mixture	Inner diameter at film surface ($d_{i,0}$) /nm [(a)]	Inner diameter along the tubes lenght ($d_{i,L}$) /nm [(b)]	Tube wall thickness (T) /nm [(b)]	Tubes length (L) /μm [(c)]
3:6:91	75 ± 12	68 ± 17	34 ± 13	8.7 ± 0.8
3:12:85	75 ± 7	78 ± 14	30 ± 5	6.3 ± 0.5
3:20:77	81 ± 6	84 ± 13	23 ± 4	5.0 ± 0.8

[(a)] From top-view FESEM images

[(b)] From TEM images

[(c)] From Confocal microscopy analysis

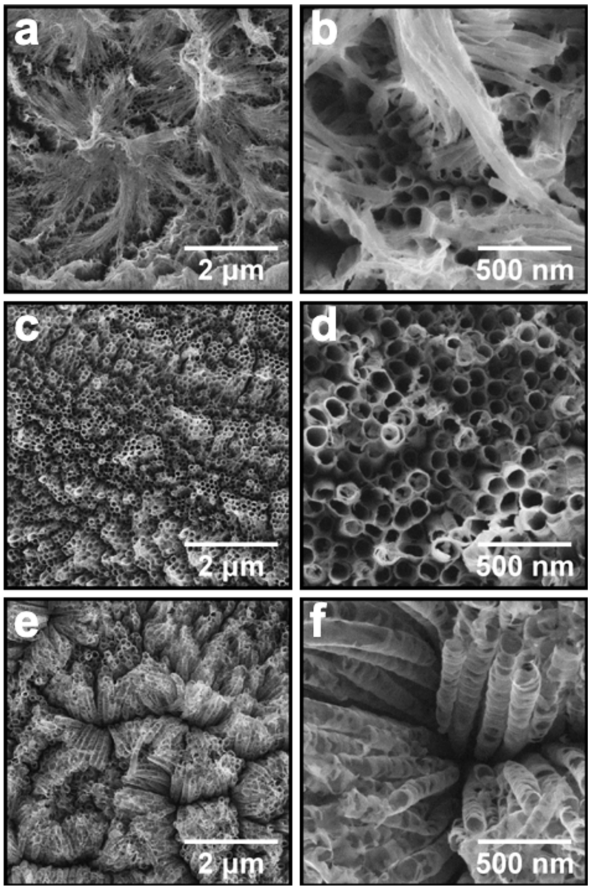

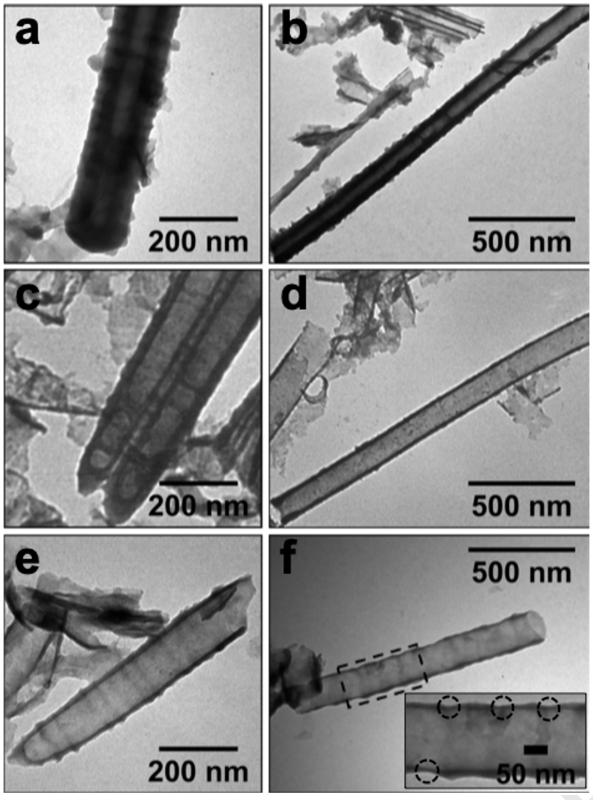

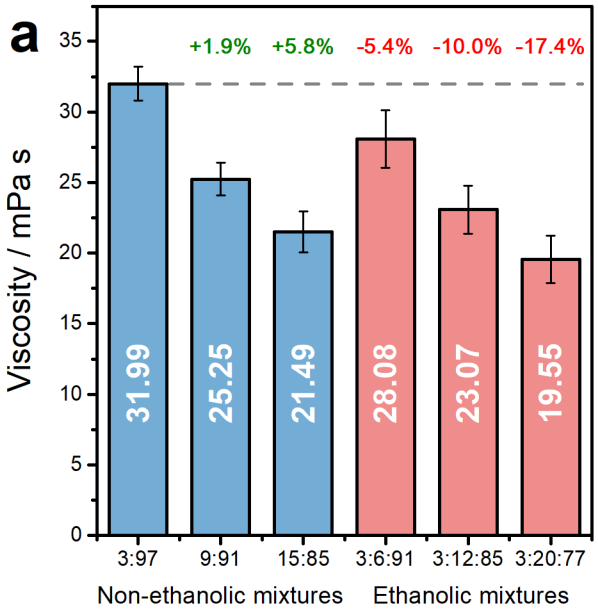
a
+1.9%
+5.8%
-5.4%
-10.0%
-17.4%
Viscosity / mPa s
31.99
25.25
21.49
28.08
23.07
19.55
3:97
9:91
15:85
3:6:91
3:12:85
3:20:77
Non-ethanolic mixtures
Ethanolic mixtures

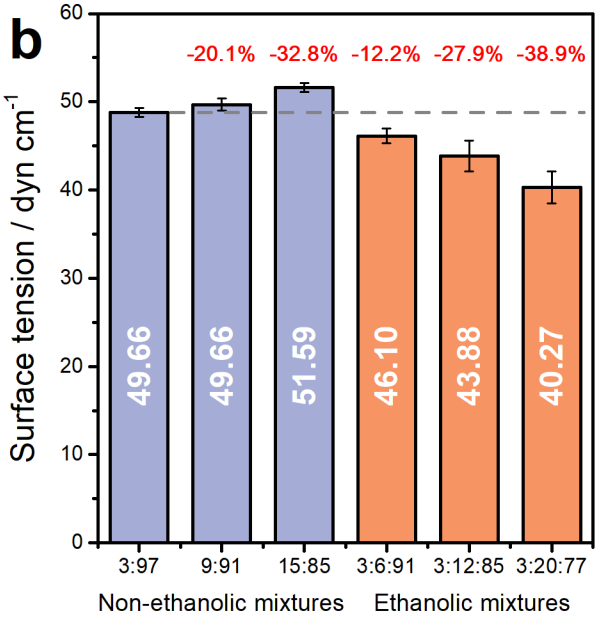
b
-20.1%
-32.8%
-12.2%
-27.9%
-38.9%
Surface tension / dyn cm-1
49.66
49.66
51.59
46.10
43.88
40.27
3:97
9:91
15:85
3:6:91
3:12:85
3:20:77
Non-ethanolic mixtures
Ethanolic mixtures

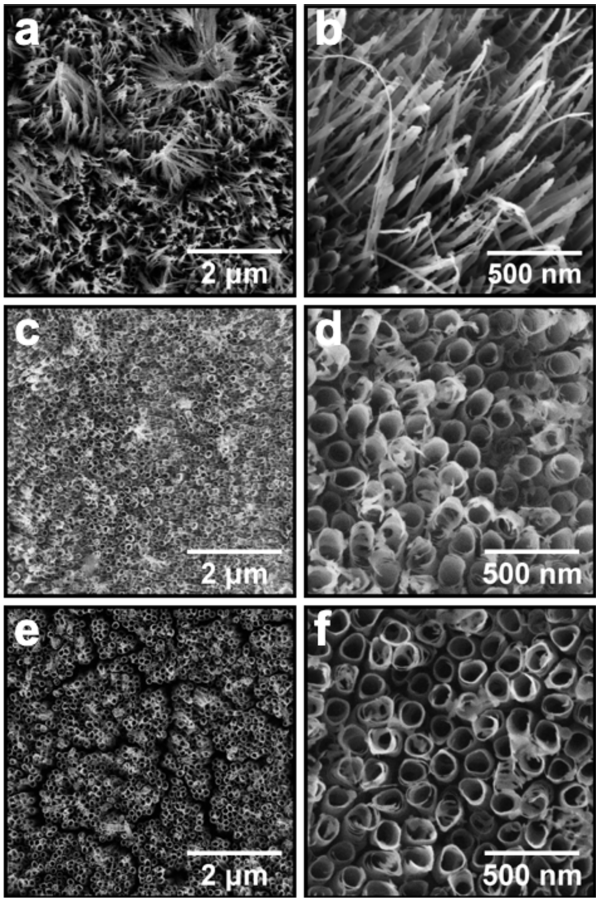

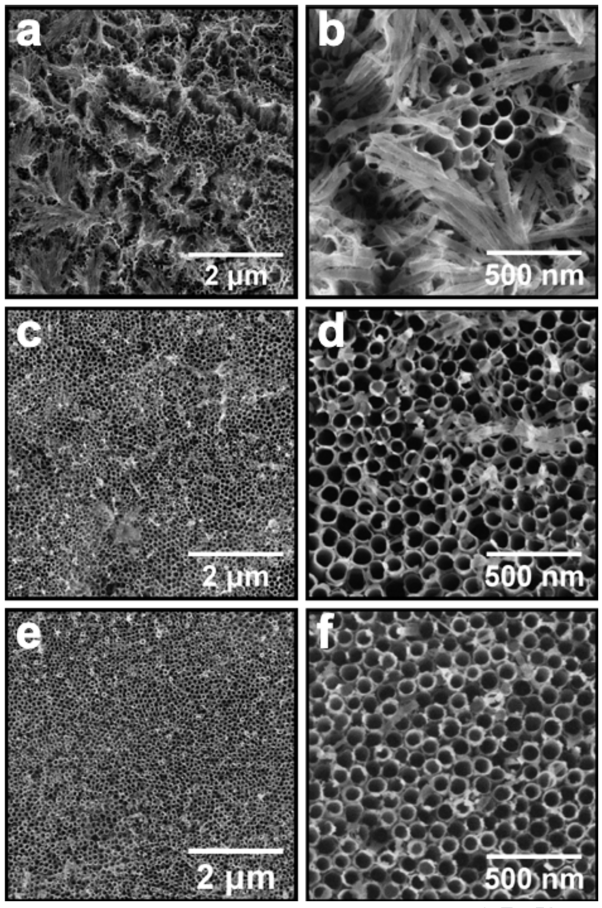

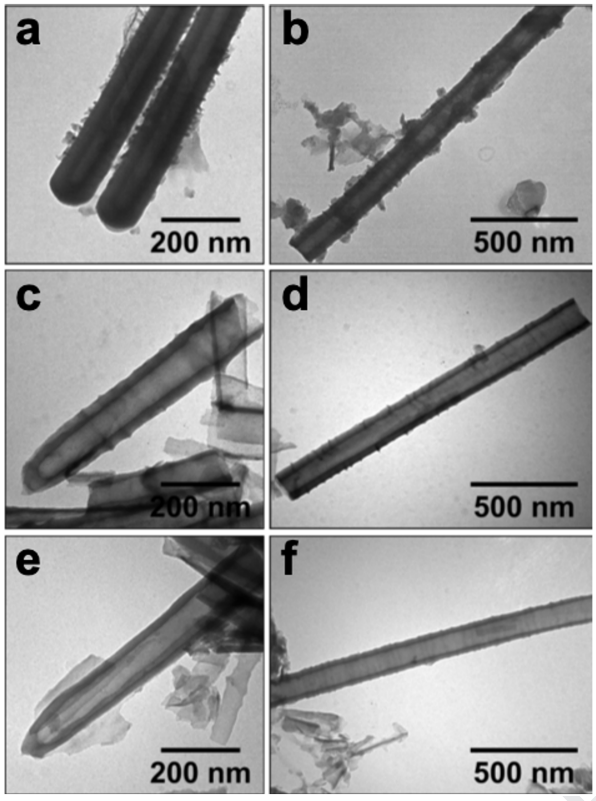

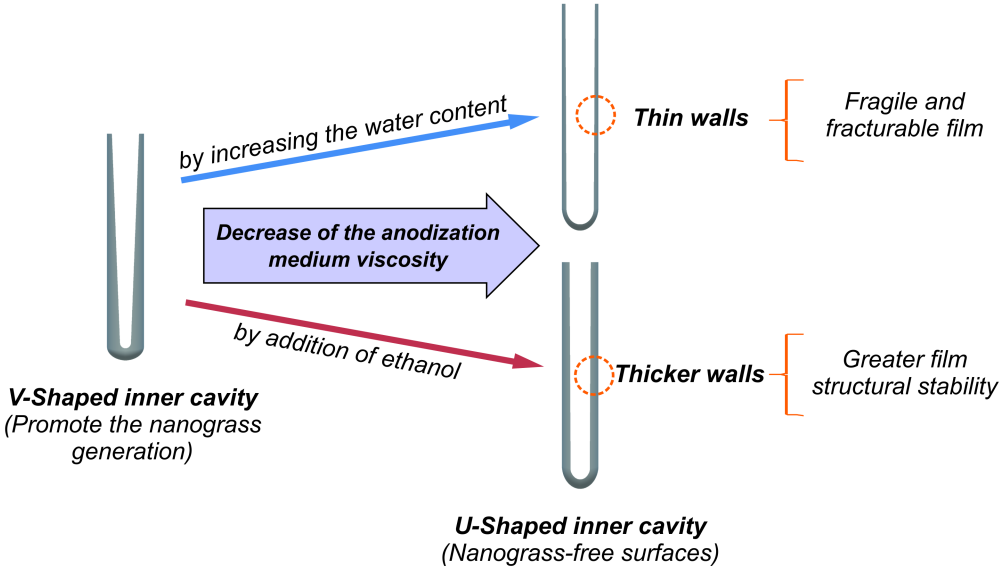

Declaration of interests

☒ The authors declare that they have no known competing financial interests or personal relationships that could have appeared to influence the work reported in this paper.

☐The authors declare the following financial interests/personal relationships which may be considered as potential competing interests: